Resolution Enhancement of Incomplete Thermal Data of Earth by Exploitation of Temporal and Spatial Correlation

Paolo Addesso, Maurizio Longo and Rocco Restaino

Dipartimento di Ingegneria dell'Informazione,
Ingegneria Elettrica e Matematica Applicata
Università degli Studi di Salerno
Via Giovanni Paolo II, 132 I-84084 Fisciano (SA), Italy
Email: {paddesso, longo, restaino}@unisa.it

Gemine Vivone

North Atlantic Treaty Organization (NATO)
Science and Technology Organization (STO)
Centre for Maritime Research and Experimentation
I-19126 La Spezia, Italy
Email: vivone@cmre.nato.int

***Abstract*—Many remote sensing applications require the availability of radiometric surface temperature information with both high acquisition rate and high spatial resolution, but unfortunately this requirement is still not achievable through a single sensor. However, the huge amount of remote sensed data provided by several heterogeneous spaceborne sensors allows to use data fusion in order to overcome this issue. In this paper, we propose a method for sharpening thermal images in a nearly real-time scenario, also capable to deal with missing data due to cloudy pixels. Moreover, we analyze the robustness of the method with respect to cloud mask misclassifications and assess its effectiveness via numerical simulations based on SEVIRI (Spinning Enhanced Visible and InfraRed Imager) data.**

Keywords–Thermal Sharpening; Cloud Masking; Multitemporal Analysis; Bayesian Smoothing; Robustness.

I. INTRODUCTION

In remote sensing applications, such as agriculture, forest management and coastal monitoring [1], remote sensed Brightness Temperature (BT) images acquired with sufficient *high temporal resolution* (*htr*) and *High Spatial Resolution* (*HSR*) could be of paramount importance. Due to physical constraints of spaceborne sensors, the strategy for achieving images with high spatial and temporal resolutions relies on fusing *low temporal resolution/High Spatial Resolution* (*ltr/HSR*) and *high temporal resolution/Low Spatial Resolution* (*htr/LSR*) data [2]. This possibility is guaranteed by the huge amount of remotely sensed data acquired by the many satellites in operation [3].

In previous research studies [4]-[6], the authors have investigated several smoothing techniques for possible use in non-real time scenarios. The most promising one relies on the fusion of images obtained by temporal interpolation of *ltr/HSR* data with others obtained by spatial interpolation of (*htr/LSR*) data (see Figure 1). This technique has the advantage of being simple enough while catching the temporal and spatial correlation that real data exhibit [7]. Unfortunately, the scenario is complicated by the presence of clouds, that is a serious issue for multitemporal techniques [8]. Simply using a cloud mask, as can be obtained via several strategies [9] [10], could not be sufficient. Indeed, the incompleteness of the images sequence may compromise the functionality and the effectiveness of most fusion algorithms. To circumvent this problem, a possible strategy is to fill the gaps in the image sequences due to clouds by estimating the BT of the cloud covered areas. Such a strategy may take advantage of the temporal correlation present in the image sequence, but must also take into account the unavoidable events of misclassified pixels. To deal with these issues, in this paper we consider several approaches to implement the said fusion strategy, focusing on different methods of spatial and temporal interpolation whose accuracy and robustness with respect to pixel misclassification in the cloud map is compared via a simulation setup based on the use of SEVIRI data [11].

The paper is organized as follows: Section II presents the formalization of thermal image sequences enhancement; Section III reports the numerical results; finally, conclusions and future developments come in Section IV.

II. METHOD DESCRIPTION

As stated before, the BT of the ground surface is masked by the top of cloud, thus contaminating the data. The solution we propose (depicted in Figure 1) relies on the availability of sufficiently accurate cloud masks, both for htr/LSR and ltr/HSR data, and is described by the following steps.

1) *Temporal Interpolation* (*TI*): the first step is applied to both the htr/LSR sequence $\mathcal{L} = \{\mathbf{L}_k : k \in T_L\}$ and the ltr/HSR sequence $\mathcal{H} = \{\mathbf{H}_k : k \in T_H\}$.

- 1.1) $\mathcal{H} = \{\mathbf{H}_k : k \in T_H\}$ is upsampled to the same time resolution of $\mathcal{L} = \{\mathbf{L}_k : k \in T_L\}$ and the cloudy pixels are estimated via a TI algorithm to obtain a sequence $\widehat{\mathcal{H}} = \{\widehat{\mathbf{H}}_k : k \in T_L\}$ (see, e.g., images $\mathbf{H}_4$ and $\widehat{\mathbf{H}}_4$ in Figure 1);
- 1.2) cloudy pixels in $\mathcal{L} = \{\mathbf{L}_k : k \in T_L\}$ are estimated via a TI operator $I_T(\cdot)$ to obtain a sequence $\widetilde{\mathcal{L}} = \{\widetilde{\mathbf{L}}_k : k \in T_L\}$ (see $\mathbf{L}_k$ and $\widetilde{\mathbf{L}}_k$ for $k = \{2, 3, 4\}$ in Figure 1).

2) *Spatial Interpolation* (*SI*): $\widetilde{\mathcal{L}} = \{\widetilde{\mathbf{L}}_k : k \in T_L\}$ is upsampled to the same spatial resolution of $\mathcal{H}$ via an SI operator $I_S(\cdot)$ to obtain the sequence $\{\widehat{\mathbf{L}}_k : k \in T_L\}$. In our setup, we choose to use a bicubic interpolator $\mathcal{B}(\cdot)$.

3) *Data Fusion*: in this step the two intermediate sequences $\widehat{\mathcal{L}}$ and $\widehat{\mathcal{H}}$ are combined, instant by instant, to obtain the estimated sequence $\mathcal{E} = \{\mathbf{E}_k : k \in T_E\}$, where, for sake of simplicity, $T_E = T_L$. More in detail, two fusion sub-steps are performed.

- 3.1) *Sharpening Fusion* (*SF*): the two intermediate sequences $\widehat{\mathcal{L}}$ and $\widehat{\mathcal{H}}$ are combined, instant by instant,

 ISBN: 978-1-61208-548-7

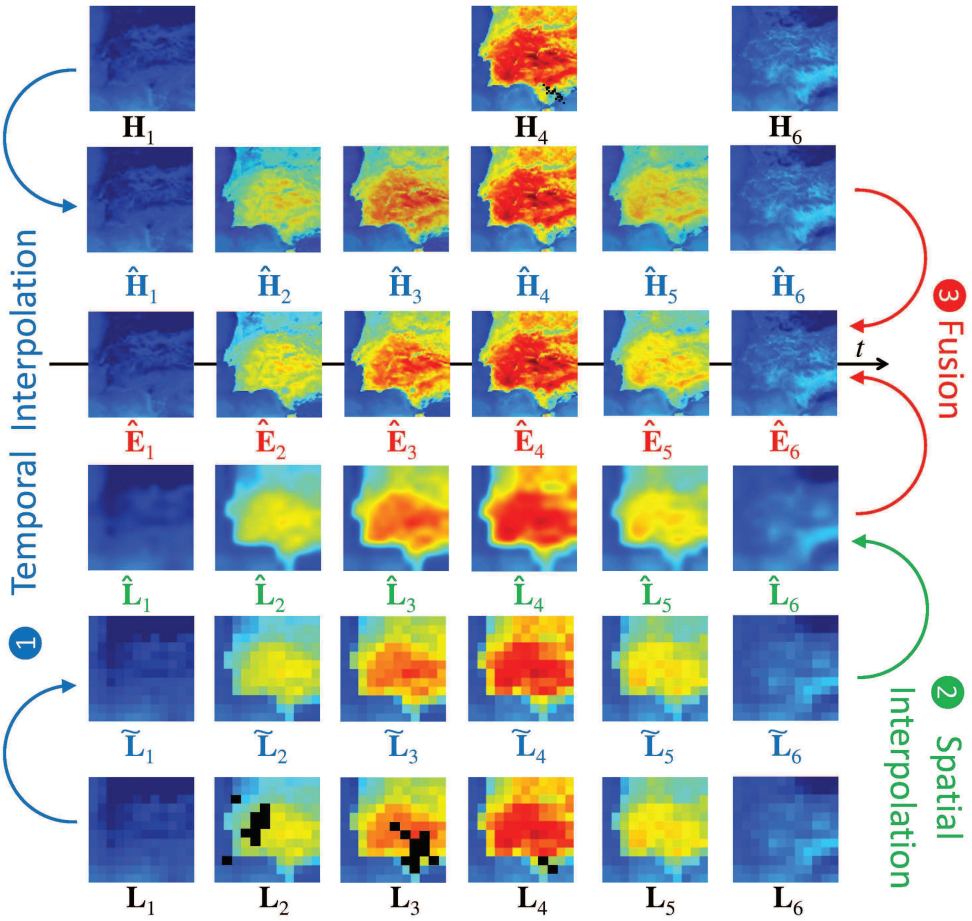

Figure 1. Pre-processing steps for BT enhancement. The image sequences are: $\{\mathbf{L}_k\}$ =*htr/LSR*, $\{\widetilde{\mathbf{L}}_k\}$ = temporal interpolation of *htr/LSR*, $\{\mathbf{H}_k\}$ = *ltr/HSR*, $\{\widetilde{\mathbf{H}}_k\}$ = temporal interpolation of *ltr/HSR*, $\{\widehat{\mathbf{L}}_k\}$ = spatial interpolation of *htr/LSR*, $\{\mathbf{E}_k\}$ = target *htr/HSR*. Dark spots in images $\mathbf{H}_4$ and $\mathbf{L}_2$,$\mathbf{L}_3$,$\mathbf{L}_4$ are the cloudy pixels.

through a sharpening rule $F_S(\cdot,\cdot)$, producing the estimate of an htr/HSR sequence $\mathcal{S} = \{\mathbf{S}_k : k \in T_L\}$. For its appealing sharpening features [12] the *High Pass Modulation* (*HPM*) (or *High Frequency Modulation - HFM*) injection scheme [13] is employed in the data fusion along with an undecimated wavelet decomposition (see also [5] for further details).

3.2) *Bayesian Smoothing* (*BS*): Bayesian smoothing allows to obtain the final estimated sequence $\mathcal{E}$ by using (for example) the *Rauch-Tung-Striebel* (*RTS*) algorithm [14], using the sharpened sequence as observation, as explained in [15].

III. Numerical Results

In this section, we consider: *i*) the accuracy of the proposed estimators in terms of Root Mean Square Error (RMSE), defined as $\sqrt{E[(\mathbf{I}-\mathbf{J})^2]}$ where $\mathbf{I}$ is the ground truth, $\mathbf{J}$ is the estimated image and $E[\cdot]$ indicates the sample average over the pixels; *ii*) the design of the TI operator $I_T(\cdot)$ under a criterion of robustness with respect to cloud masking error.

As test set, we employ sequences of thermal images acquired by the SEVIRI sensor in the band IR 10.8, characterized by the a spatial resolution of about 6 km and a temporal rate of 4 images per hour. In particular, the presented results are related to data collected on 16 August 2014 on the Iberian peninsula (latitude between 35.7 and 41.4 degrees North, longitude between 4.1 and 9.8 degrees West). The simulation setup is as follows. The original dataset plays the role of the estimating htr/HSR sequence $\mathcal{E}$. $\mathcal{H}$ is simulated by selecting a subset of $\mathcal{E}$ with a temporal interval $\Delta^H = 8$ between each couple of ltr/HSR images. $\mathcal{L}$ is simulated by generating a spatially degraded version of $\mathcal{E}$, with spatial resolution ratio $R = 6$ between $\mathcal{E}$ and $\mathcal{L}$.

Given the unavailability of a ground truth for the soil (or sea) temperature under the clouds, we use clear sky images and artificially change the BT of the whole image in order to mimic a temperature decrease which is typical when clouds are present. The top of the cloud is supposed to have a BT of 270 K, and the initial and final transition phases, modeled via a raised cosine function, are completed in 1 hour (see Figure 2, panel (a)). The time duration of each period of cloud coverage is indicated with $\Delta^c = \{2, 4\}$, and the cloudy images are chosen to be in the midpoints between two HSR images, that are the most critical point for our algorithms. More in detail:

 ISBN: 978-1-61208-548-7

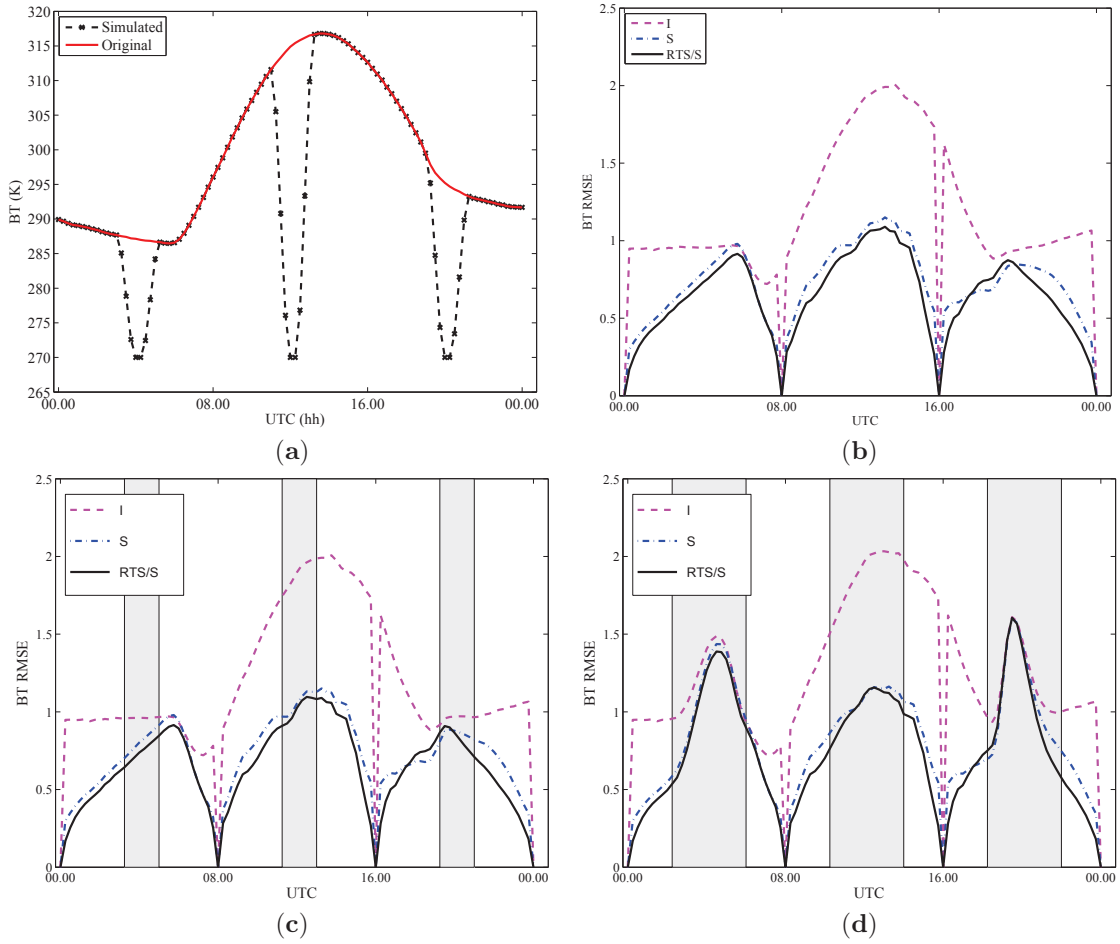

Figure 2. Panel **(a)**: BT time evolution for cloud simulation (black dashed line) and original data (red continuous line) when $\Delta^c = 2$ hh. Panels **(b)**-**(d)**: RMSE computed between the forecast of thermal SEVIRI image and the actual value for the simulated Spain dataset in the PCC case. The panel **(b)** refers to the case in which the clouds are absent. Panels **(c)** and **(d)** refer to cloud data periods (highlighted by the gray-shaded areas) with time duration $\Delta^c = 2$ hh and $\Delta^c = 4$ hh respectively.

TABLE I. RMSE RELATED TO SIMULATED PCC SCENARIOS. RELEVANT PARAMETERS ARE $R = 6$ AND $\Delta^H = 8$ hh.

	Type	Δ^c [h]	I	S	RTS/S
Whole	Cloud	2	1.251	0.759	**0.697**
	Cloud	4	1.332	0.883	**0.832**
	Clear-sky	[2,4]	1.249	0.756	**0.692**
Cloudy	Cloud	2	1.346	0.916	**0.875**
	Clear-sky	2	1.337	0.905	**0.859**
	Cloud	4	1.475	1.099	**1.061**
	Clear-sky	4	1.319	0.887	**0.834**

- when $\Delta^c = 2$ hours, we put the cloud coverage in the intervals $[03.00 - 05.00]$, $[11.00 - 13.00]$ and $[19.00 - 21.00]$ UTC (Universal Time Coordinated);
- when $\Delta^c = 4$ hours, we put the cloud coverage in the intervals $[02.00 - 06.00]$, $[10.00 - 14.00]$ and $[18.00 - 22.00]$ UTC.

The approach has been assessed in two cases: *i*) *Perfect Cloud Classification* (*PCC*), in which perfect cloud/no cloud pixel classification is assumed; *ii*) *Non Perfect Cloud Classification* (*NPCC*), in which misclassifications are considered.

A. Perfect Cloud Classification

In the scenario of error-free cloud mask, we use a *TI* scheme based on a blockwise Cubic Interpolation (CI) to compute $\widetilde{\mathcal{L}}$ and $\widetilde{\mathcal{H}}$ sequences and then we compare the following three algorithms.

- *Interpolated image estimation* (*I*): this method is used as a yardstick, since it does not involve any data fusion (the estimate at time k is given by the bicubic interpolation bicubic interpolation of the LSR sequence $\widehat{\mathcal{L}} = I_S(\widetilde{\mathcal{L}})$).
- *Sharpened image estimation* (*S*): The estimate at time k is produced by performing a *SF*, as described in Sect. II, namely it coincides with the sequence $\mathcal{S} = F_S(\widehat{\mathcal{L}}, \widetilde{\mathcal{H}})$.

 ISBN: 978-1-61208-548-7

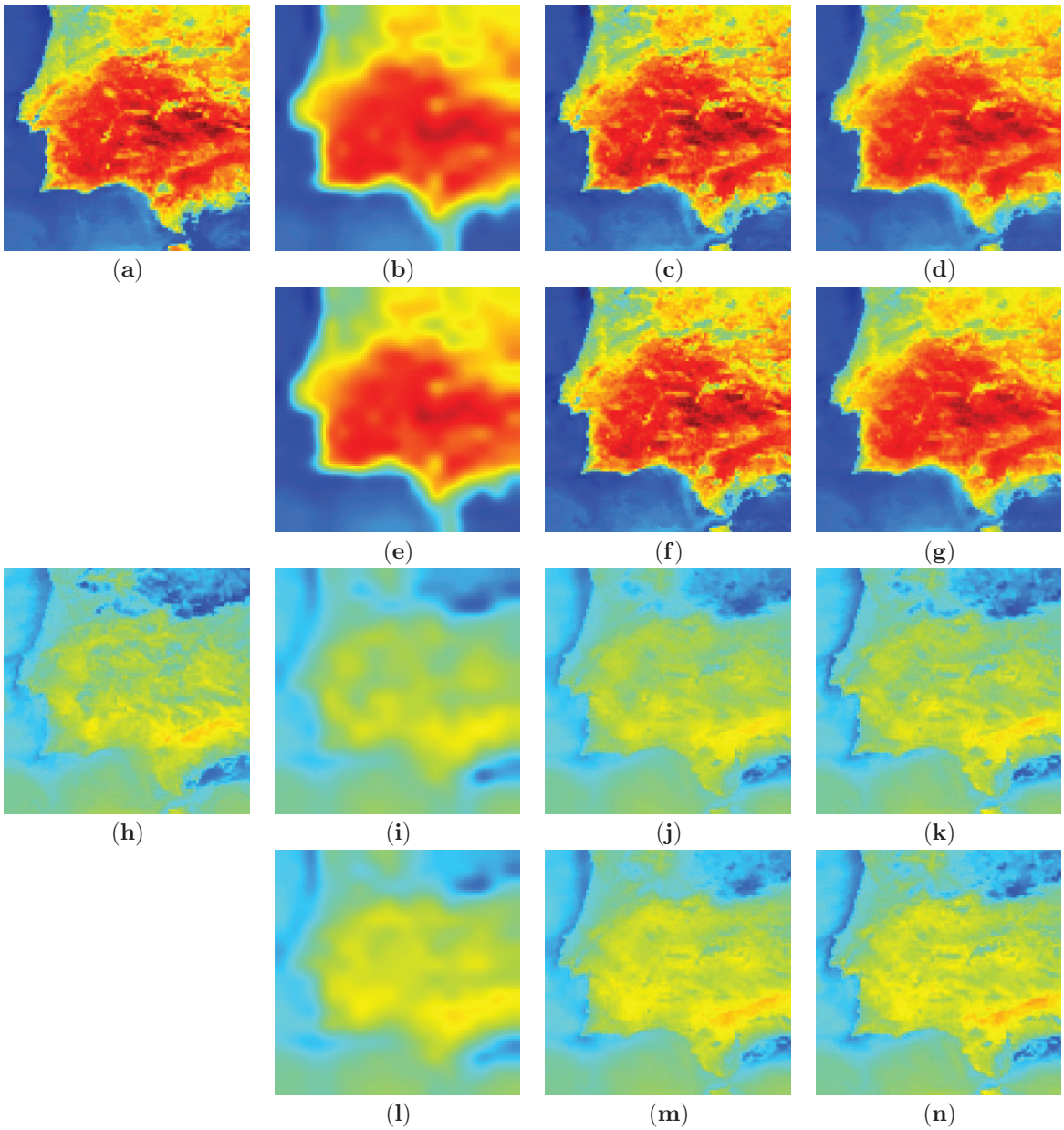

Δ^c	t = 12.00 UTC			t = 20.00 UTC		
	I	S	RTS/S	I	S	RTS/S
2	1.898	1.054	**1.026**	0.970	0.878	**0.864**
4	1.968	**1.099**	1.110	1.471	1.448	**1.427**

Figure 3. Example of estimation with missing data. Panel **(a)**: missing image to be estimated (acquired at 12.00 UTC on 16 August 2014). Panels **(b)**-**(d)**: images estimated at 12.00 UTC on 16 August 2014 for $\Delta^c = 2$ by algoritms I **(b)**, SI **(c)** and RTS/S **(d)**. Panels **(e)**-**(g)**: images estimated at 12.00 UTC on 16 August 2014 for $\Delta^c = 4$ by algoritms I **(e)**, SI **(f)** and RTS/S **(g)**. Panel **(h)**: missing image to be estimated (acquired at 20.00 UTC on 16 August 2014). Panels **(i)**-**(k)**: images estimated at 20.00 UTC on 16 August 2014 for $\Delta^c = 2$ by algoritms I **(i)**, SI **(j)** and RTS/S **(k)**. Panels **(l)**-**(n)**: images estimated at 20.00 UTC on 16 August 2014 for $\Delta^c = 4$ by algoritms I **(l)**, SI **(m)** and RTS/S **(n)**. At the bottom, RMSE values for the estimated images.

 ISBN: 978-1-61208-548-7

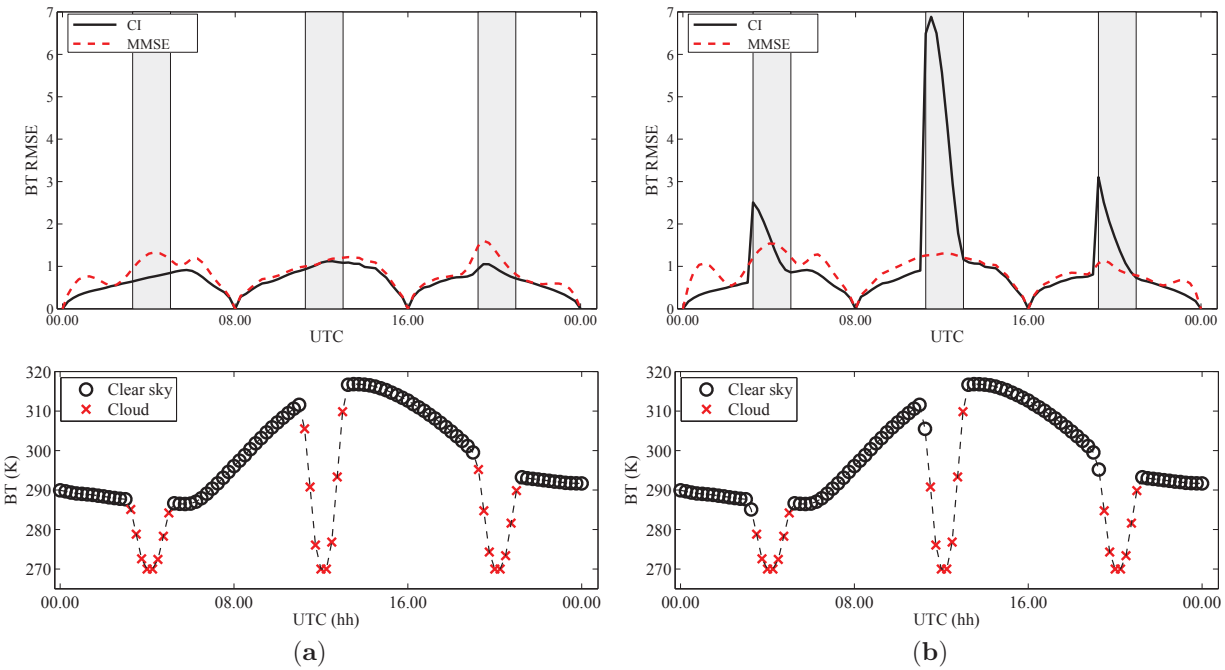

Figure 4. RMSE computed between the forecast of thermal SEVIRI image and the actual value for the simulated Spain dataset (top plots) and related cloud mask (bottom plots). The gray-shaded areas in top plots are referred to the true cloud data periods with time duration $\Delta^c = 2$ hh. The panel **(a)** refers to PCC case, while the panel **(b)** refers to NPCC case.

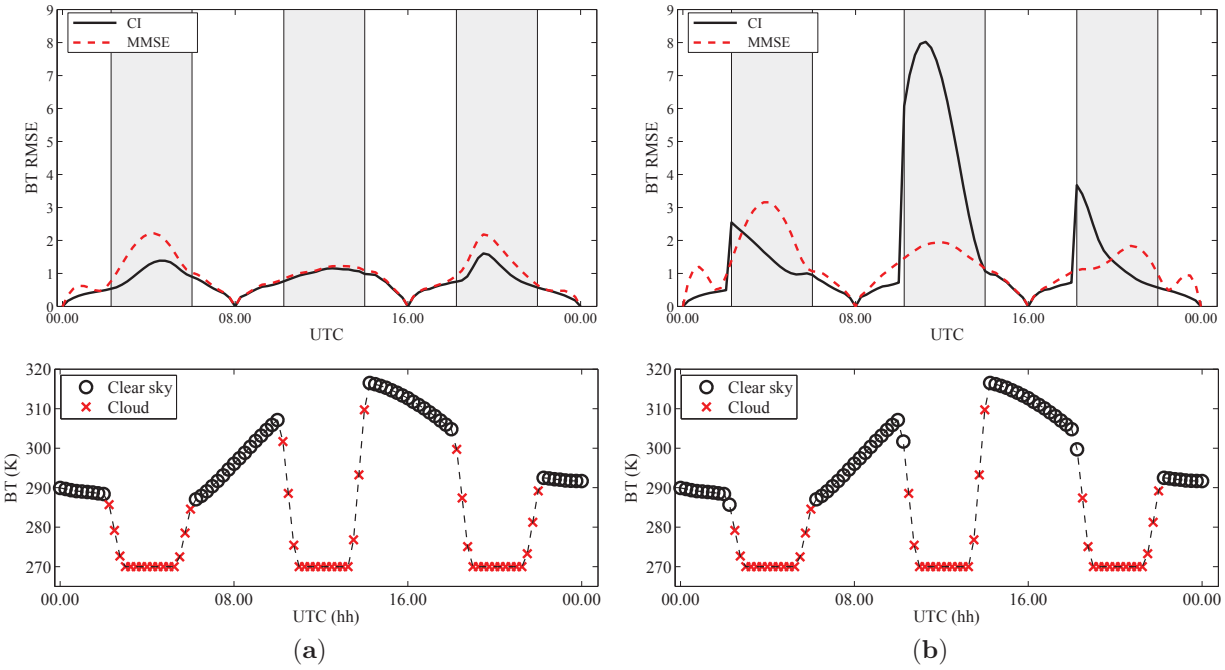

Figure 5. RMSE computed between the forecast of thermal SEVIRI image and the actual value for the simulated Spain dataset (top plots) and related cloud mask (bottom plots). The gray-shaded areas in top plots are referred to the true cloud data periods with time duration $\Delta^c = 4$ hh. The panel **(a)** refers to PCC case, while the panel **(b)** refers to NPCC case.

- *RTS smoother with Sharpened observation* (*RTS/S*): in this method, we employ a *BS* algorithm, i.e., the RTS one, that is fed by observations constructed upon the sharpened images.

The results are summarized in Figures 2-3 and in Table I. More in detail, in Figure 2, plots (c) and (d), it is shown the RMSE vs. time for the cases $\Delta^c = 2$ hours and $\Delta^c = 4$ hours, respectively. We can see that the error in estimating the htr/HSR sequence slightly increases in the first case during missing data intervals (i.e., the gray-shaded areas), with respect to the case without missing data (i.e., Figure 2, plot (b)), while the performance significantly degrades for $\Delta^c = 4$.

The performance trend is made evident looking at the RMSEs in Table I, computed over all time frames (Whole) and over the cloudy frames only (Cloudy), and more precisely comparing over the HSR images estimated in the cloudy frames (Type = "Cloud") with the RMSEs of the HSR images estimated in the same frames when no clouds have been added (Type = "Clear-sky"). Finally, in Figure 3 we present some image useful for a visual appreciation of the effectiveness of both the S algorithm and (even more) the RTS/S algorithm in producing satisfactory estimated HSR images (Figure 3, panels (c) and (d) for $\Delta^c = 2$ and panels (f) and (g) for $\Delta^c = 4$), in comparison with the missing HSR original image (Figure 3, panel (a)) acquired at 12.00 UTC. A similar comparison can be carried out looking at panels (i)-(n) of Figure 3, that are the estimated HSR images of a missing HSR original image (Figure 3, panel (h)) acquired on the same area, in the same day, but at 20.00 UTC. In any case, in the average, the best algorithm is RTS/S because it is the most stable one, though it is not uniformly the best one in every instance.

B. Non Perfect Cloud Classification

In dealing with the effects of cloud/no cloud misclassification, but limiting ourselves to the RTS/S rule, we focus on two possible *TI* interpolation strategies: (i) CI and (ii) MMSE, namely a polynomial fitting obtained via a Minimum Mean Square Error.

The results are summarized in Figure 4 and Figure 5 that refers to the cases $\Delta^c = 2$ hh and $\Delta^c = 4$ hh respectively. We can see that CI strategy outperforms MMSE one in PCC case, but it is less robust than MMSE when a single cloudy pixel is misclassified, as shown in panel **(b)** of both Figure 4 and Figure 5. Note also that the misclassification of a clear-sky pixel (not shown in this contribution) is by far less dangerous, because both techniques are not very sensitive to this kind of error, as evident by the analysis carried out in the previous subsection. Accordingly, these results give some hints for the design of the cloud detection algorithm, that should aim to minimize the probability of a miss.

IV. Conclusion

High spatial resolution thermal maps, collected with an elevate acquisition rate, are often required for several applications about the monitoring of rural and urban areas. In this paper, we present a framework that is able to perform a non real-time sharpening of thermal images encompassing the presence of missing data. It combines techniques of temporal smoothing and spatial enhancement by taking advantage of a Bayesian smoother relied upon the Rauch-Tung-Striebel algorithm and a pansharpening method belonging to the multi-resolution analysis family (an undecimated wavelet decomposition with a high pass modulation injection scheme). The experimental results using real data acquired by the SEVIRI sensor (band IR 10.8) demonstrate the ability of the proposed approach to reach better performance with respect to techniques based on either temporal interpolation or spatial sharpening and, in particular, the ability of the proposed technique to deal with missing data (e.g. due to the presence of clouds).

This work deserves further investigations towards the introduction of *a priori* knowledge about the surface (such as its Digital Elevation Model) or of the physical model of the incoming solar radiation.

References

[1] W. Zhan, Y. Chen, J. Zhou, J. Li, and W. Liu, "Sharpening thermal imageries: A generalized theoretical framework from an assimilation perspective," IEEE Trans. Geosci. Remote Sens., vol. 49, no. 2, Feb. 2011, pp. 773–789.

[2] F. Gao, J. Masek, M. Schwaller, and F. Hall, "On the blending of the landsat and MODIS surface reflectance: predicting daily Landsat surface reflectance," IEEE Trans. Geosci. Remote Sens., vol. 44, no. 8, Aug. 2006, pp. 2207–2218.

[3] M. Chi et al., "Big data for remote sensing: Challenges and opportunities," Proceedings of the IEEE, vol. 104, no. 11, Nov 2016, pp. 2207–2219.

[4] P. Addesso et al., "Enhancing TIR image resolution via Bayesian smoothing for IRRISAT irrigation management project," in Proc. SPIE Remote Sensing, no. 8887, 2013, pp. 888 710–1–888 710–13.

[5] P. Addesso, M. Longo, A. Maltese, R. Restaino, and G. Vivone, "Batch methods for resolution enhancement of TIR image sequences," IEEE J. Sel. Topics Appl. Earth Observ., vol. 8, no. 7, July 2015, pp. 3372–3385.

[6] P. Addesso et al., "Robustified smoothing for enhancement of thermal image sequences affected by clouds," in IEEE Geoscience and Remote Sensing Symposium (IGARSS), 26-31 July, Milan, Italy, 2015, pp. 1076–1079.

[7] A. Kallel, C. Ottle, S. L. Hegarat-Mascle, F. Maignan, and D. Courault, "Surface temperature downscaling from multiresolution instruments based on markov models," IEEE Transactions on Geoscience and Remote Sensing, vol. 51, no. 3, March 2013, pp. 1588–1612.

[8] X. Li et al., "Recovering quantitative remote sensing products contaminated by thick clouds and shadows using multitemporal dictionary learning," IEEE Transactions on Geoscience and Remote Sensing, vol. 52, no. 11, Nov 2014, pp. 7086–7098.

[9] P. Addesso, R. Conte, M. Longo, R. Restaino, and G. Vivone, "MAP-MRF cloud detection based on PHD filtering," IEEE J. Sel. Topics Appl. Earth Observ., vol. 5, no. 3, June 2012, pp. 919–929.

[10] G. Vivone, P. Addesso, R. Conte, M. Longo, and R. Restaino, "A class of cloud detection algorithms based on a MAP-MRF approach in space and time," IEEE Trans. Geosci. Remote Sens., vol. 52, no. 8, Aug 2014, pp. 5100 – 5115.

[11] F. Pasternak, P. Hollier, and J. Jouan, "Seviri, the new imager for meteosat second generation," in Geoscience and Remote Sensing Symposium, 1993. IGARSS '93. Better Understanding of Earth Environment., International, Aug 1993, pp. 1094–1099 vol.3.

[12] G. Vivone, R. Restaino, M. Dalla Mura, G. Licciardi, and J. Chanussot, "Contrast and error-based fusion schemes for multispectral image pansharpening," IEEE Geosci. and Remote Sens. Letters,, vol. 11, no. 5, May 2014, pp. 930–934.

[13] R. Schowengerdt, Remote Sensing: Models and Methods for Image Processing, 3rd Ed. Elsevier, 2007.

[14] H. Rauch, F. Tung, and C. Striebel, "Maximum likelihood estimates of linear dynamic systems," AIAA Journal, vol. 3, no. 8, 1965, pp. 1445–1450.

[15] P. Addesso, M. Longo, R. Restaino, G. Vivone, and A. Maltese, "An interpolation-based data fusion scheme for enhancing the resolution of thermal image sequences," in IEEE Geoscience and Remote Sensing Symposium (IGARSS), 13-18 July, Quebec, Canada, 2014, pp. 4926–4929.

 ISBN: 978-1-61208-548-7